

Relaxation of thermo-remanent magnetization in Fe-Cr GMR multilayers

R. S. Patel and A. K. Majumdar*

Department of Physics, Indian Institute of Technology, Kanpur-208 016, India

A. K. Nigam

*Tata Institute of Fundamental Research,
Homi Bhabha Road, Mumbai-400 005, India*

(Dated: November 16, 2018)

Abstract

The time decay of the thermo-remanent magnetization (TRM) in Fe-Cr giant magnetoresistive (GMR) multilayers has been investigated. The magnetization in these multilayers relaxes as a function of time after being cooled in a small magnetic field of 100 Oe to a low temperature and then the magnetic field is switched off. Low-field (< 500 Oe) magnetization studies of these samples have shown hysteresis. This spin-glass-like behavior may originate from structural imperfections at the interfaces and in the bulk. We find that the magnetization relaxation is logarithmic. Here the magnetic viscosity is found to increase first with increasing temperature, then it reaches a maximum around T_g , and then it decreases with increasing temperature. This behavior is different from that of conventional spin glasses where the logarithmic creep rate is observed to increase with temperature. Power law also gives good fits and it is better than the logarithmic fit at higher temperatures. The dynamical effects of these multilayers are related to the relaxation of thermally blocked superparamagnetic grains and magnetic domains in the film layers.

PACS numbers: 75.70.Cn, 75.50.Lk, 76.60.Es, 75.10.Nr

Keywords: Thermoremanence, Magnetization, Spin glass, Fe-Cr multilayers

*Electronic address: akm@iitk.ac.in

I. INTRODUCTION

In Fe-Cr GMR multilayers the ferromagnetic (FM) Fe layers are exchange coupled through the non-magnetic Cr spacer layers. An antiferromagnetic arrangement of the Fe layers is engineered by varying Cr spacer layer thickness. With varying Cr thickness successive Fe layers show oscillatory antiferromagnetic (AFM) and FM couplings but with decreasing peak coupling strength. It is believed that in an external magnetic field $H > H_{sat}$, the magnetization in the Fe layers are aligned as in a ferromagnetic material but in the absence of the magnetic field they are in antiferromagnetic configuration. Our study is focussed at finding the magnetic relaxation of these multilayers in low external magnetic fields (~ 100 Oe).

Thermoremanent magnetization is a thermally activated process. When the applied magnetic field is removed the magnetization tries to approach the remanent magnetization value in order to minimise the energy of the system. A magnetic system has dipolar energy, anisotropy energy, and exchange energy. In general, ferromagnetic materials do not respond to the magnetic fields immediately. There is a time lag between the application/withdrawal of the magnetic field and the response of magnetization to the field. This phenomenon is called “magnetic viscosity” [1]. Folks and Street [2] described this time lag by domain processes which progress through states of metastable equilibrium to a stable state. The major domain processes are:

1. coherent or incoherent rotation of magnetization in single domain particles,
2. pinning and unpinning of domain boundary walls, and
3. nucleation of domains of reverse magnetization.

Coherent rotation of magnetization vector and the Bloch-wall formation are primary consequences of lowering energy after the external field is applied/removed. Thermal agitation plays an important role in transition from metastable to stable states. One may ask what are the time scales to achieve stable states for paramagnetic, FM, and AFM materials. What is the role of magnetic interaction and crystal structure in the time dependence of magnetization?

Dahlberg et al. [3] explained the time dependence as a consequence of interactions or couplings. The interaction between relaxing spins, the dipole coupling, drives the system from

an initial state towards the equilibrium state. They attributed the strong time dependence of the magnetization in Co-Cr films to the demagnetization in the film.

Sinha [4] et al. found that in $Fe_{80-x}Ni_xCr_{20}$ ($x = 30$, FM phase) $M(t)$ fits well to the power law decay. They found that with the increase of wait time, the exponent becomes smaller. For $x = 14$ (AF phase) also, power law decay describes $M(t)$ quite well and the exponent decreases with increasing temperature. Chamberlin [5] studied EuS which is considered to be an ideal Heisenberg FM system with a Curie temperature ~ 16.6 K. They found that the plots of remanent magnetization versus logarithm of time show negative curvature for $T < T_B (= 17.75$ K) and exhibits an S-shaped curve for $T > T_B$. Ulrich et al. [6] studied the magnetic relaxation of single domain ferromagnetic particles below the blocking temperature. They found that for all particle densities the relaxation decays following a power law, with density-dependent exponent and a temperature-dependent prefactor. They used Monte Carlo simulations to study the influence of dipolar interactions and polydispersion on the magnetic relaxation of single-domain FM particles below the blocking temperature. They concluded (i) stretched exponential decay at low densities, (ii) a power law decay at intermediate densities, and (iii) relaxation toward a non-vanishing remanent magnetization at high densities.

In an earlier study of $Cu_{100-x}Mn_x$ ($x = 76, 83$ and both in AF phase) we found [7] that the power law decay is better at lower temperatures. The fits at a given temperature improve with stronger long-range antiferromagnetic order (AF1 structure). Leighton and Schuller [8] used time-dependent magnetization measurements to probe the asymmetry in the magnetization reversal mechanism in exchange-biased MnF_2/Fe bilayers. They found that on one side of the loop, coherent rotation of magnetization plays an important role while on the other side the domain nucleation. The time dependence of the magnetization on the coherent rotation side of the loop had a form that is consistent with a small distribution of energy barriers. The side of the loop characterised by domain nucleation and propagation shows a logarithmic time dependence with a field dependent viscosity. Similar investigation was also carried by Fullerton and Bader [9] on Fe/FeSi multilayers.

Chamberlin et al. [10] studied the time decay of the thermoremanent magnetization in 1.0 % CuMn and 2.6 % AgMn spin glasses. They found it to be a stretched exponential function. Till that time no data had been published supporting an algebraic decay (power law) for magnetization. Chamberlin also [11] found that the effect of wait-time t_w can be empirically

characterised as an exponential decrease of the relaxation frequency with increasing wait time. If the sample is allowed to remain in the field-cooled state long enough before the field is removed, then the magnetization will not relax: a spin glass can have a permanent magnetization in zero field. Chubykalo and Gonzalez [12] simulated the relaxational behavior of Co-Ni multilayers with different layer thickness. Their simulations had shown that the thermally activated demagnetization process in Co-Ni multilayers does not occur according to the Arrhenius kinetics. Panagiotopoulos et al. [13] found that the magnetic relaxation follows the $\ln(t)$ behavior at 5 K in La-Ca-Mn-O FM/AF multilayer with $T_B = 70$ K. In FM films that exhibit a wide range of energy barriers the magnetization time decay follows a $\ln(t)$ behavior only below a blocking or freezing temperature, resulting from the superposition of many exponential decays with different magnetic relaxation times. Chen et al. [14] found that the magnetization relaxation of a $[Co_{80}Fe_{20}(1.4nm)/Al_2O_3(3nm)]_{10}$ sample obeys a power-law decay of the thermoremanent magnetic moment with an asymptotic remanence when starting from a completely relaxed FC state.

Street and Brown [15] described two types of mechanisms that are responsible for the time dependence in ferromagnetic materials known as “diffusion” and “fluctuation” after-effect or viscosity. Chantrell et al. [16] gave a phenomenological theory based on the intrinsic energy barrier to explain the form of time dependence of the magnetization. The slow relaxation is related to the irreversible magnetic behavior via a fictitious fluctuation field H_f which itself determines a quantity called the activation volume V_{act} . Both H_f and V_{act} are related to the magnetization reversal process. For granular materials V_{act} is generally smaller than the grain size. A simple model for the time dependence of the switching field in magnetic recording media by Sharrock [17] accounts for thermally assisted crossing of an energy barrier whose height is reduced by the applied field. Goodman et al. [18] studied a system with a narrow distribution of energy barriers. In such systems, at fields less than the coercive field, an accelerating variation of magnetization with log of time is seen and a decelerating behavior of field above the coercivity. In the coercive field region an ‘S’ shaped variation is observed.

II. EXPERIMENTAL DETAILS

Our samples were grown on Si substrates by ion beam sputter deposition technique using Xe ion at 900 V with beam current of 20 mA and 1100 V with beam current of 30 mA. The typical structures are Si/Cr(50 Å)/[Fe(20 Å)/Cr(t Å)] \times 30/Cr(50 - t Å). Samples 1 - 4 have $t = 6, 8, 10$ and 12 Å, respectively. Samples 1 and 2 are deposited at 900 V and samples 3 and 4 are at 1100 V. Our multilayers show a GMR ($= ((\rho(H, T) - \rho(0, T))/\rho(0, T)) \times 100\%$) of $\approx 1, 33, 20$ and 21 % at 4.2 K for an external field of ≈ 1 tesla (H_{sat}). These samples are well characterised and the details have been given elsewhere[19]. All the experiments were done with a Quantum Design superconducting quantum interference device (SQUID) magnetometer(MPMS). A magnetic field of 100 Oe is applied in the plane of the multilayer samples at 300 K and the sample is cooled down to the measuring temperature. After the temperature is stabilised, the magnetic field is set to zero and $M(T)$ measurements were started and continued till 12,000 s.

III. THEORY

Chamberlin [22] summarised the time dependence of magnetization in terms of different mathematical expressions as follows:

1. The most popular empirical expression for characterising amorphous materials has been the Kohlrausch-Williams-Watts stretched exponential $M(t) \propto \exp(-(t/\tau)^\beta)$.
2. For crystals, the Curie-von Schweidler power law $M(t) \propto t^{-\beta}$.
3. For magnetic aftereffects, the Neèl logarithmic time dependence $M(t) \propto \log(t/\tau)$ is popular.

When the applied magnetic field is removed, the magnetization takes finite time to cross the energy barrier for reversal. If the energy barriers are identical then the magnetic moment M is given by [8]

$$M(t) = A + B \exp(-t/\tau_0), \tag{1}$$

where

$$\frac{1}{\tau_0} = f_0 \exp\left(\frac{E_A}{k_B T}\right),$$

A and B are constants, t represents the elapsed time, f_0 is the attempt frequency, E_A is the activation energy, and T is the measurement temperature. When there is a distribution of barriers, then

$$M(t) = M_0 - S \ln(t). \quad (2)$$

Here S is called the “magnetic viscosity” and M_0 is a constant at a given measuring field. S is expected to reach a peak value near the coercive field H_c where the rate of change of the moment with time reaches the maximum. The intermediate case with a small distribution of barrier heights is more complicated to quantify.

Power-law behavior is predicted by scaling theories for domain growth and internal dynamics [5]. Calculations based on Sherrington-Kirkpatrick mean-field model suggest that the magnetization decays algebraically as

$$M(t) = M_0 t^{-\beta}. \quad (3)$$

Other treatments yield Kolrausch-Williams-Watts stretched-exponential relaxation which is common in spin-glass like systems [22] given by

$$M(t) = M_0 \exp\left(-\left(\frac{t}{\tau}\right)^n\right). \quad (4)$$

When measured in a small static field, the temperature dependence of the magnetization of a spin glass changes abruptly at the glass transition temperature (T_g). Above T_g the magnetization obeys the Curie-Weiss law, attributable to weakly interacting paramagnetic spins whereas below T_g the magnetization is cooling history dependent. If it is field cooled then the magnetization is nearly independent of temperature below T_g ; if it is zero-field cooled then the magnetization increases with increasing temperature.

IV. RESULTS AND DISCUSSION

Structure-wise our samples are a good combination of crystalline layers of ferromagnetic Fe and antiferromagnetic Cr and the polycrystalline interfaces. So these samples provide a complicated combination of crystalline layers and polycrystalline interfaces consisting of ferromagnetic, antiferromagnetic and spin-glass like structures as shown schematically in Fig. 1. In this figure black and grey spheres represent Cr and Fe atoms, respectively. Directions of the arrow show the direction of spin alignment. Typical estimates of the relative strengths of the Fe-Fe, Fe-Cr, and Cr-Cr couplings are 1 : -0.3 : -0.18 [20] and 1 : -0.55 : -0.3 [21]. In other words, Fe-Fe coupling is FM and Fe-Cr & Cr-Cr couplings are AF. Fe-Fe coupling is two/three times stronger than Fe-Cr coupling. ‘?’ in Fig. 1 represents uncertainty of spin direction (frustration) at that site. For a particular direction, either it will be violating the FM Fe-Fe coupling or the AF Fe-Cr coupling. As the Fe-Fe coupling is stronger than the Fe-Cr and Cr-Cr coupling most of the frustration occurs at Cr sites (black spheres). Attempts to explain magnetic relaxation with mathematical expressions began a century back. We have made a similar attempt to understand the response of the combined system for small magnetic fields. Although Chamberlin[22] argued that these empirical expressions are simple mathematical formulae that give generally good agreement with a wide variety of measurements but demonstrating agreement with these formulae tells nothing about the mechanism of response.

For our analysis, we have used a standard non-linear least-squares-fit program. Here χ^2 is defined as

$$\chi^2 = \frac{1}{N} \sum_{i=1}^N \frac{(M_{i-measured} - M_{i-fitted})^2}{M_{i-mean}^2}. \quad (5)$$

In our multilayer system, the ferromagnetic Fe layers have in-plane magnetization but as they are not super-lattices, there will be some domain like structures in the ferromagnetic plane with distribution of domain volume. Thus we expect that there is a distribution of barriers for which logarithmic relaxation of magnetization is generally found. So we first tried the logarithmic fit in the form of Eq. (2). For our analysis we have taken data from 100 s to 12,000 s. We have made measurements with a SQUID magnetometer and it takes \sim 10 s to make one measurement and a much longer time to achieve stability and equilibrium condition after removal of the magnetic field. So we have not analysed the data for $t < 100$ s.

Logarithmic relaxation gives excellent fits for samples 2 - 4 with correlation coefficients ~ 0.997 and the normalised χ^2 consistent with the experimental resolution of one part in 10^4 . For sample 1, which has the least GMR, the fit is not so good ($R^2 \sim 0.90$). Figures 2, 3, and 4 show the raw M vs. $\ln t$ data and the fits for samples 2, 3, and 4, respectively at different temperatures. For each sample, M_0 decreases with increasing temperature which can be understood as the decrease in magnetization due to thermal fluctuations. The coefficient S , which is termed as the magnetic viscosity, initially increases linearly with temperature; then it decreases at higher temperatures. Larger S implies larger change in the magnetization during the observational time period. S shows a peak around T_g of the ZFC magnetization curves (samples 2 - 4 show T_g at $\sim 62, 123,$ and 83 K, respectively taken at 100 Oe [23]). This can be understood as follows: At temperatures much lower than the freezing temperature, due to the low temperature (less thermal energy), the magnetic moments can not relax much (as they are nearly frozen). So lower the temperature lower is the value of S . At temperatures much higher than the freezing temperature, due to higher thermal energy the system behaves more and more like a paramagnetic/superparamagnetic system. In the paramagnetic region the entire magnetization relaxes very rapidly (<10 s)[10]. So in our measurement time window ($10^2 - 10^4$ s) we hardly observe any relaxation and hence S looks small. At around T_g in the ZFC magnetization curve, the thermal energy provides the moments freedom to move and they can also interact with one another. In this region, the system is like a spin glass which is about to unfreeze and so the magnetization responds much faster. That is why we find maxima in the magnetic viscosity vs. temperature curves. This is shown in Fig. 5. To make the comparison more clear we have shown the percentage change in magnetization with time at different temperatures for sample 2 in Fig. 6. Similar variation of S with temperature was found by Guy [24] in a Au-Fe spin-glass alloy containing 2 at. % Au. However, Lottis et al. [25] found broad maxima in the temperature dependence of S in Co-Cr films.

Figure 7 shows the raw M vs. $\ln t$ data and the fit for sample 1. Sample 1 showed the least GMR. The interpretation for the least GMR is that in this sample with Cr thickness of 6 \AA most Fe layers are coupled ferromagnetically to the neighbouring Fe layers. So the whole sample is like a FM material. The ZFC magnetization measurements of this sample show that the magnetization decreases monotonically with increasing temperature. So measurement temperatures of $50, 100,$ and 150 K are much above the T_B of this sample.

The magnetization, plotted on a logarithmic scale, has clearly an ‘S’- shape as shown in Fig. 7.

Next we tried to fit the data to the power law in the form of Eq. (3). We find that the power law gives equally good fits for samples 2 - 4, with $R^2 > 0.99$ along with χ^2 consistent with the experimental resolution. The numerical value of the parameter β is the same as of the parameter ‘S’ divided by M_0 of Eq. (2). We can rewrite Eq. (3) as

$$M(t) = M_0 t^{-\beta} = M_0(e^{-\beta \ln(t)}) \approx M_0 - (M_0\beta) \ln(t), \quad (6)$$

since β is very small and so we can neglect higher order terms. This has a form similar to that of Eq. (2). For larger time scale $t > 10^5$ s, $t^{-\beta}$ decreases faster than $\ln(t)$. We have tried to show this feature in Fig. 8. In other words, from our measurement time window we shall not be able to distinguish log and power fits. However, a careful observation from Tables I-IV indicates a small difference between the two fits. Eq. (2) gives better fit than Eq. (3) at low temperatures but at higher temperatures (much above T_g) Eq. (3) gives better fits. Sample 1 does not have T_g or T_B in the measured temperature range and so the power law fit is better for all the temperatures. A stronger proof would have been possible if we could take data till $10^5 - 10^6$ s.

Next we tried the stretched exponential fit in the form of Eq. (4). The low-field magnetization measurements on samples 2-4 had shown spin-glass-like history dependent behaviour. But this fitting gave unrealistic large time constants (τ) with equally large errors.

To conclude, in these sputtered GMR multilayers which are structural combinations of FM Fe films, AF Cr Films, and Fe-Cr mixed interfaces, the magnetization decays logarithmically at low temperatures and above T_g the magnetization decays algebraically. In the multilayers one expects less distribution of energy barriers but we could not find any exponential decay. For ‘AFM’ (sample 2, 3, and 4) and ‘FM’ (sample 1) multilayers we found different decay mechanisms. The power law decay is better at higher temperatures. It is difficult to distinguish between ‘good AFM’ (sample 2 with GMR of 33 %) and ‘AFM’ (sample 3 with GMR of 21 % and sample 4 with GMR of 20 %) samples from their decay behavior.

Acknowledgments

We sincerely thank Drs. D. Temple and C. Pace of MCNC, Electronic Technologies Division, Research Triangle Park, North Carolina for providing us the samples. One of us (R.S.P.) acknowledges CSIR, Government of India, for financial support.

- [1] R. Street and J. C. Woolley, Proc. Phys. Soc. London Sec. A **62**, 562 (1949).
- [2] L. Folks and R. Street, J. Appl. Phys. **76**, 6391 (1994).
- [3] E. Dan Dahlberg, D. K. Lottis, R. M. White, M. M. Matson, and E. Engle, J. Appl. Phys. **76**, 6401 (1994).
- [4] G. Sinha, R. Chatterjee, M. Uehara, and A. K. Majumdar, J. Magn. Magn. Mater. **164**, 345 (1996).
- [5] R. V. Chamberlin and F. Holtzberg, Phys. Rev. Lett. **67**, 1606 (1991).
- [6] M. Ulrich, J. Garcia-Otero, J. Rivas, and A. Bunde, Phys. Rev. B **67**, 024416 (2003).
- [7] R. S. Patel, D. Kumar, and A. K. Majumdar, Phys. Rev. B **66**, 054408 (2002).
- [8] C. Leighton and Ivan K. Schuller, Phys. Rev. B **63**, 174419 (2001).
- [9] E. E. Fullerton and S. D. Bader, Phys. Rev. B **53**, 5112 (1996).
- [10] R. V. Chamberlin, G. Mozurkewich, and R. Orbach, Phys. Rev. Lett. **52**, 867 (1984).
- [11] R. V. Chamberlin, Phys. Rev. B **30**, R5393 (1984).
- [12] O. A. Chubykalo, J. M. Gopez, J. Magn. Magn. Mater. **196-197**, 810 (1999).
- [13] I. Panagiotopoulos, N. Moutis, and C. Christides, Phys. Rev. B **65**, 132407 (2002).
- [14] X. Chen, W. Kleemann, O. Petravic, O. Sichelshmidt, S. Cardoso, and P. P. Freitas, Phys. Rev. B **68**, 054433 (2003).
- [15] R. Street and S. D. Brown, J. Appl. Phys. **76**, 6386 (1994).
- [16] R. W. Chantrell, A. Lyberatos, M. El-Hilo, and K. O'Grady, J. Appl. Phys. **76**, 6407 (1994).
- [17] M. P. Sharrock, J. Appl. Phys. **76**, 6413 (1994).
- [18] A. M. Goodman, H. Laidler, K. O'Grady, N. W. Owen, and A. K. Petford-Long, J. Appl. Phys. **87**, 6409 (2000).
- [19] J. M. Lannon Jr., C. C. Pace, D. Temple G. E. McGuire, A. F. Hebard, and M. Ray, Materials Research Society Symposium - Proceedings, **690**, 157 (2002).

- [20] Z. P. Shi and R. S. Fishman, *Phys. Rev. Lett.* **78**, 1351 (1997).
- [21] A. Berger and E. E. Fullerton, *J. Magn. Magn. Mater.* **121**, 471 (1997).
- [22] R. V. Chamberlin, *J. Appl. Phys.* **76**, 6401 (1994).
- [23] R. S. Patel, A. K. Majumdar, A. K. Nigam, D. Temple, and C. Pace, [arXiv:cond-mat/0504275](https://arxiv.org/abs/cond-mat/0504275).
- [24] C. N. Guy, *J. Phys. F: Metal Phys.*, **8**, 1309 (1978).
- [25] Daniel K. Lottis, E. Dan Dahlberg, J. A. Christner, J. I. Lee. R. L. Peterson, and R. M. White, *J. Appl. Phys.*, **63**, 2920 (1988).

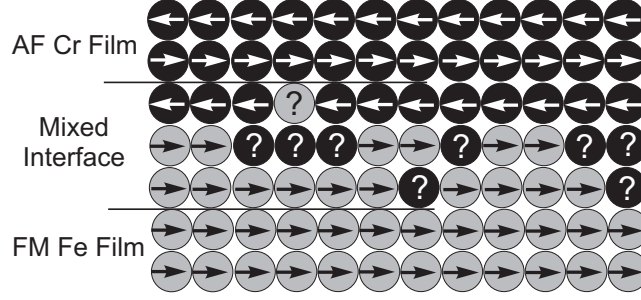


FIG. 1: Schematic diagram of the sputtered GMR samples. Black and grey spheres represent Cr and Fe atoms, respectively. Typical estimates of the relative strengths of the Fe-Fe, Fe-Cr, and Cr-Cr couplings are $1 : -0.3 : -0.18$ [20] and $1 : -0.55 : -0.3$ [21]. Directions of the arrow show the spin alignment direction. “?” shows the uncertainty (frustration) in the spin direction at that site.

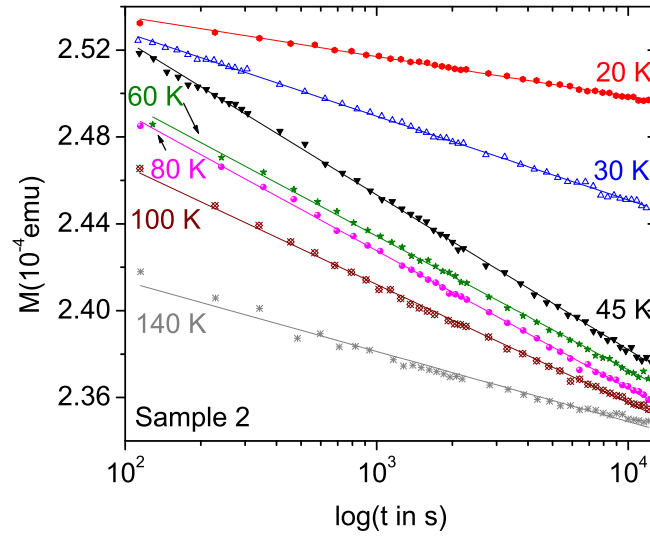


FIG. 2: (Color online) M (raw data) is plotted against $\log(t \text{ in s})$ for sample 2. The solid lines are the logarithmic fits to Eq. (2). The data and the fits are multiplied by 1.285, 1.66, 1.73, 2.27, 2.85, and 3.92 for 30, 45, 60, 80, 100, and 140 K, respectively to show all the curves on the same figure.

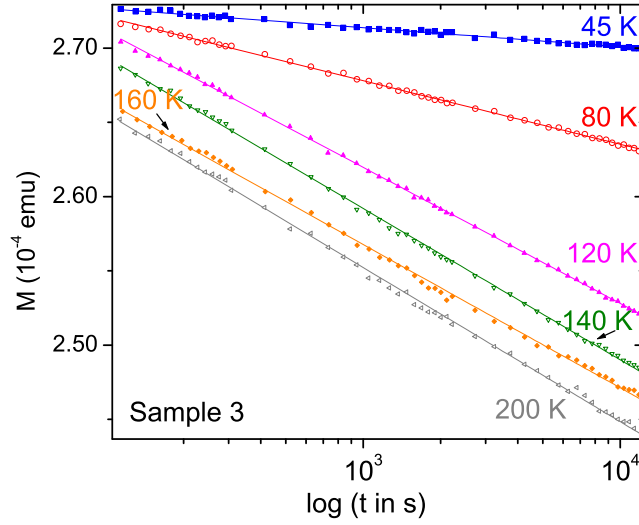


FIG. 3: (Color online) M (raw data) is plotted against $\log(t \text{ in s})$ for sample 3. The solid lines are the logarithmic fits to Eq. (2). The data and the fits are multiplied by 1.3, 2.3, 3.2, 4.42, and 8.4 for 80, 120, 140, 160, and 200 K, respectively to show all the curves on the same figure.

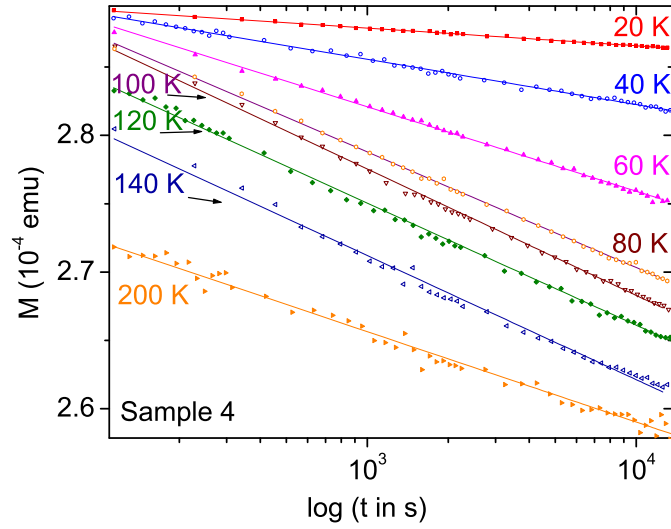


FIG. 4: (Color online) M (raw data) is plotted against $\log(t \text{ in s})$ for sample 4. The solid lines are the logarithmic fits to Eq. (2). The data and the fits are multiplied by 1.19, 1.45, 1.9, 2.5, 3.45, 4, and 8.2 for 40, 60, 80, 100, 120, 140, and 200 K, respectively to show all the curves on the same figure.

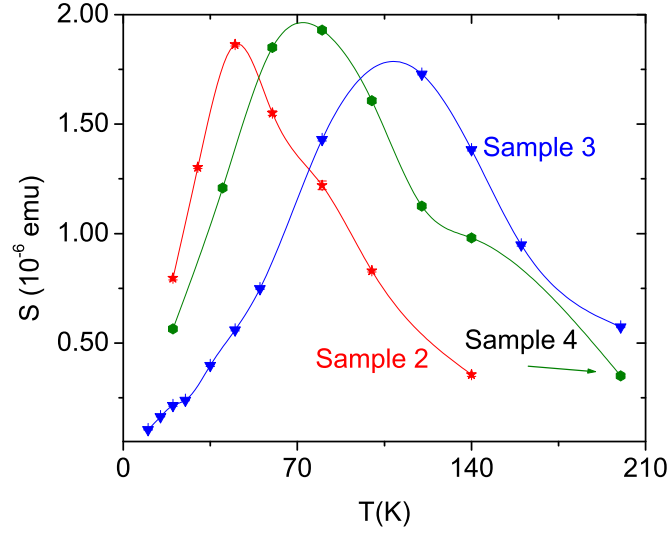


FIG. 5: (Color online) Variation of the parameter S of Eq. (2) with temperature. The solid lines are just guides to the eye.

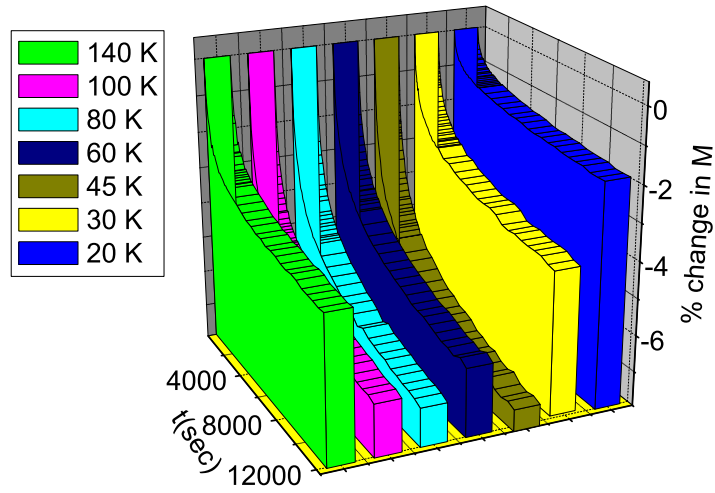


FIG. 6: (Color online) Percentage change in M is plotted against t (s) at various temperatures for sample 2.

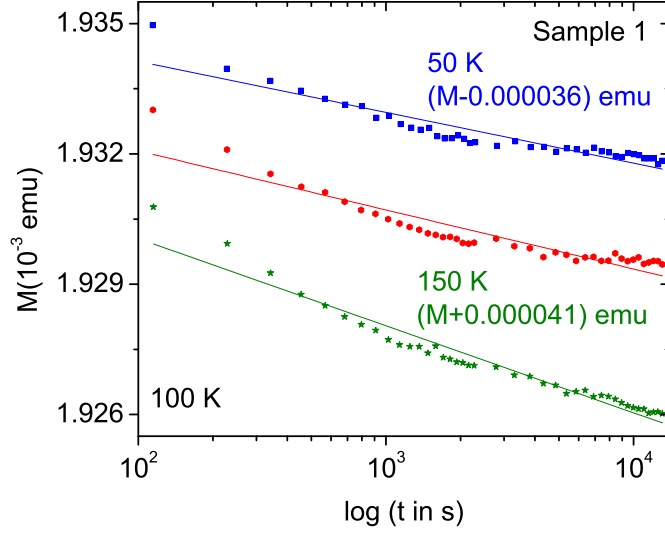


FIG. 7: (Color online) M (raw data) is plotted against $\log(t \text{ in s})$ for sample 1. The solid lines are the logarithmic fits to Eq. (2). The data and the fits for 50 and 150 K are shifted along y-axis for clarity.

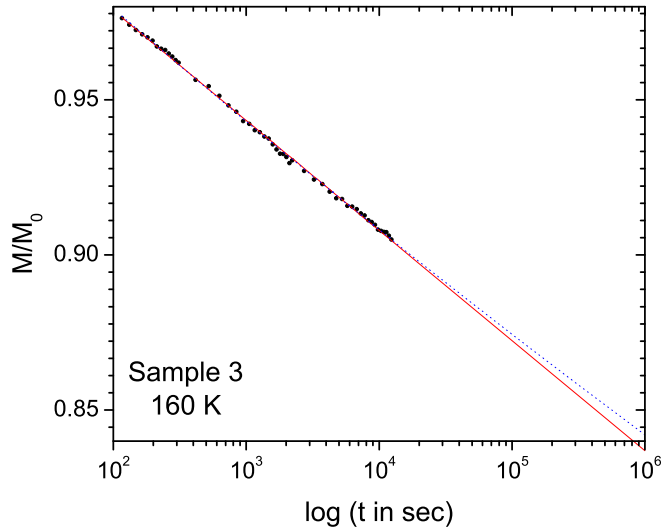


FIG. 8: (Color online) M/M_0 is plotted against $\log(t \text{ in s})$ for sample 3 at 160 K. The solid line is the logarithmic fit to Eq. (2) and the dashed line is the power fit to Eq. (3). Both the fits are extended till 10^6 s to show that in larger time window the power fit decreases slower than the logarithmic fit. However, in our measurement time span there is only a small difference between the two fits.

TABLE I: Values of χ^2 , correlation coefficient R^2 , the parameters M_0 , S of Eq. (2), M_0 , and β of Eq. (3) for sample 1.

T(K)	$\chi^2(10^{-8})$	R^2	$M_0(10^{-5}emu)$	$S(10^{-7}emu)$
50	1.407	0.8778	197.24 ± 0.02	5.1 ± 0.3
100	2.110	0.8707	193.48 ± 0.03	5.9 ± 0.3
150	1.713	0.9497	189.30 ± 0.02	8.7 ± 0.3
T(K)	$\chi^2(10^{-8})$	R^2	$M_0(10^{-5}emu)$	$\beta(10^{-4})$
50	1.405	0.8779	197.00 ± 0.02	2.6 ± 0.2
100	2.108	0.8708	193.00 ± 0.03	3.1 ± 0.2
150	1.709	0.9498	189.00 ± 0.02	4.6 ± 0.2

TABLE II: Values of χ^2 , correlation coefficient R^2 , and the parameters M_0 , S of Eq. (2), M_0 , and β of Eq. (3) for sample 2.

T(K)	$\chi^2(10^{-8})$	R^2	$M_0(10^{-5}emu)$	$S(10^{-7}emu)$
20	5.1674	0.9965	25.721 ± 0.006	7.96 ± 0.08
30	11.621	0.9988	20.274 ± 0.004	13.03 ± 0.06
45	29.432	0.9992	16.066 ± 0.006	18.64 ± 0.07
60	25.028	0.9986	15.140 ± 0.008	15.5 ± 0.1
80	20.487	0.9895	11.54 ± 0.01	12.2 ± 0.2
100	24.683	0.9983	9.037 ± 0.004	8.30 ± 0.05
140	89.531	0.9833	6.320 ± 0.006	3.56 ± 0.08
200	1119.8	0.9969	1.698 ± 0.004	6.21 ± 0.06
T(K)	$\chi^2(10^{-8})$	R^2	$M_0(10^{-5}emu)$	$\beta(10^{-3})$
20	5.4684	0.9963	25.727 ± 0.006	3.17 ± 0.03
30	12.7867	0.9987	20.296 ± 0.005	6.74 ± 0.03
45	36.7689	0.999	16.126 ± 0.007	12.65 ± 0.05
60	29.2681	0.9983	15.187 ± 0.009	11.06 ± 0.07
80	22.0195	0.9988	11.570 ± 0.006	11.41 ± 0.06
100	19.4450	0.9987	9.059 ± 0.004	9.86 ± 0.06
140	88.8819	0.9834	6.328 ± 0.006	5.9 ± 0.1
200	1807.83	0.995	1.7690 ± 0.007	48.3 ± 0.6

TABLE III: Values of χ^2 , correlation coefficient R^2 , the parameters M_0 , S of Eq. (2), M_0 , and β Eq. (3) for sample 3.

T(K)	$\chi^2(10^{-8})$	R^2	$M_0(10^{-5}emu)$	$S(10^{-7}emu)$
10	15.52408	0.9872	26.223 ± 0.002	1.04 ± 0.02
15	17.2138	0.9944	25.8571 ± 0.002	1.64 ± 0.02
20	63.2449	0.9885	25.5907 ± 0.003	2.15 ± 0.04
25	44.2073	0.9930	26.2994 ± 0.003	2.39 ± 0.03
35	87.8776	0.9954	34.2492 ± 0.004	3.97 ± 0.04
45	12.3645	0.9872	27.525 ± 0.007	5.60 ± 0.09
55	54.5099	0.9993	22.8914 ± 0.002	7.47 ± 0.03
80	12.2490	0.9989	21.588 ± 0.005	14.3 ± 0.07
120	16.2190	0.9997	12.584 ± 0.003	17.29 ± 0.04
140	36.9160	0.9994	9.056 ± 0.003	13.83 ± 0.05
160	75.9658	0.9988	6.464 ± 0.003	9.48 ± 0.05
200	84.3582	0.9988	3.409 ± 0.002	5.37 ± 0.03
T(K)	$\chi^2(10^{-8})$	R^2	$M_0(10^{-5}emu)$	$\beta(10^{-3})$
10	0.3085	0.9872	29.814 ± 0.002	0.397 ± 0.004
15	0.3483	0.9944	29.398 ± 0.002	0.635 ± 0.008
20	1.2901	0.9884	29.096 ± 0.003	0.85 ± 0.02
25	0.8924	0.9930	29.901 ± 0.003	0.92 ± 0.02
35	1.8190	0.9953	28.847 ± 0.004	1.58 ± 0.02
45	12.3258	0.9872	27.527 ± 0.007	2.06 ± 0.03
55	1.1379	0.9993	26.034 ± 0.003	3.35 ± 0.02
80	13.4735	0.9988	21.613 ± 0.005	6.95 ± 0.03
120	22.8617	0.9996	12.652 ± 0.004	15.24 ± 0.04
140	26.3087	0.9996	9.116 ± 0.003	17.15 ± 0.05
160	56.4284	0.9991	6.504 ± 0.003	16.39 ± 0.07
200	5296.38	0.9456	3.364 ± 0.001	15.0 ± 0.4

TABLE IV: Values of χ^2 , correlation coefficient R^2 , and the parameters M_0 , S of Eq. (2), M_0 , and β of Eq. (2) for sample 4.

T(K)	$\chi^2(10^{-8})$	R^2	$M_0(10^{-5}emu)$	$S(10^{-7}emu)$
20	1.8586	0.9969	29.175 ± 0.004	5.64 ± 0.05
40	20.7856	0.9969	24.832 ± 0.007	12.08 ± 0.09
60	27.4387	0.9980	20.73 ± 0.01	18.5 ± 0.1
80	28.9706	0.9989	16.007 ± 0.008	19.3 ± 0.1
100	49.0388	0.9985	12.212 ± 0.008	16.07 ± 0.1
120	103.588	0.9981	8.749 ± 0.005	11.25 ± 0.05
140	248.365	0.9925	7.46 ± 0.01	9.8 ± 0.1
200	346.956	0.9883	3.481 ± 0.004	3.50 ± 0.05
T(K)	$\chi^2(10^{-8})$	R^2	$M_0(10^{-5}emu)$	$\beta(10^{-3})$
20	26.4418	0.9955	2.9180 ± 0.0005	1.97 ± 0.02
40	20.4407	0.9969	2.4848 ± 0.0007	5.05 ± 0.04
60	33.6017	0.9976	2.078 ± 0.001	9.58 ± 0.07
80	33.0043	0.9988	1.608 ± 0.001	13.28 ± 0.07
100	32.6814	0.9990	1.2280 ± 0.0007	14.62 ± 0.07
120	79.7989	0.9985	0.8793 ± 0.0005	14.22 ± 0.07
140	194.536	0.9942	0.750 ± 0.001	14.7 ± 0.2
200	333.72	0.9887	0.3492 ± 0.0004	10.9 ± 0.1